



# Development of a Modular Multilevel Cascade Converter Based on Full-Bridge Submodules with a Common DC Bus

João Rego<sup>1</sup>(✉), Fábio Lúcio Pereira<sup>1</sup>, Luis A. M. Barros<sup>1,2</sup>, António P. Martins<sup>3</sup>, and J. G. Pinto<sup>1,2</sup>

<sup>1</sup> Department of Industrial Electronics, University of Minho, Guimarães, Portugal  
a81341@uminho.pt

<sup>2</sup> Centro ALGORITMI, University of Minho, Guimarães, Portugal

<sup>3</sup> SYSTEC Research Center, University of Porto, Porto, Portugal

**Abstract.** The Modular Multilevel Cascade Converters (MMCC) present themselves as one of the solutions for high power and high voltage applications. Modularity and low voltage stress in each semiconductor are some of the features of this solution. This paper presents a study with experimental results concerning an MMCC composed by three full-bridge submodules with a common DC-bus and with low frequency cascaded transformers. Sharing the DC bus for each submodule allows for a simpler control algorithm as well as a simpler interface point with renewable energy sources or energy storage systems. Along the paper, it is presented the step-by-step methodology to obtain the main parameters of the elements that constitute the MMCC, namely the transformers equivalents model. Thus, it was possible to develop a more realistic simulation model, whose results obtained are very similar to the experimental results.

**Keywords:** Modular multilevel cascade converter (MMCC) · Cascade transformers · Simulation model

## 1 Introduction

The increasing technological evolution combined with the increase in electrical energy demand encourages the investigation of more efficient and effective power conversion solutions. In this sense, power electronic converters have been gaining popularity due to their versatility and features. The evolution of power semiconductors has led to the appearance of more robust and compact topologies for power electronic converters. Two and three-level DC-AC power electronic converters are the most widely used topologies. These power converters are used in several applications, such as interfacing renewable energy sources with the power grid, driving electric motors, charging electric vehicles, and other applications [1, 2]. Regarding the control, they are usually controlled by Pulse Width Modulation (PWM) technique. As such, the output harmonic content is dispersed, which causes high losses in the system, namely in the output passive filters

[1]. Furthermore, the semiconductors have a higher volt-age stress [1, 3]. For that reason, conventional converters are not feasible for high power and high voltage applications.

The Multilevel Converter (MLC), namely the Modular Multilevel Converter (MMC) and the Modular Multilevel Cascaded Converter (MMCC) concepts, presents themselves as innovative solutions to mitigate the mentioned problems. The MMCC allows the connection of different submodules, being the number of added submodules adjusted in order to withstand the desired voltage. The more submodules added, the more voltage levels the MMCC can synthesize [1]. Consequently, it is possible to obtain a waveform closer to the sinusoidal one, which minimizes the harmonic spectrum, being more concentrated on the fundamental component and the switching frequency [1, 4]. Therefore, it is possible to reduce the  $dv/dt$  variations at the output, allowing the integration of smaller passive filters and more robust semiconductors [1]. For these reasons, system losses are lower, and the efficiency is higher, which is important for high power applications [1, 5–8]. In [1] and in [9] it is possible to conclude the impact of the number of levels that the MMCC can synthesize on the out-put signals, both in the time domain and in the frequency domain. With a smaller number of voltage levels, the harmonic spectrum is wide and with considerable amplitude values. On the other hand, with a higher number of voltage levels, the harmonic spectrum is more concentrated in the fundamental frequency and switching frequency, having reduced amplitudes along the rest of the harmonic spectrum. This feature facilitates the design of passive filters. In [9], the influence of the modulation index on the number of levels that an MMCC composed of cascaded full-bridge can synthesize was studied. The total harmonic distortion (THD) has a higher value for low voltage levels.

Due to lower voltages in each submodule, the voltage stress is reduced. Furthermore, with the integration of MMCC based solutions, it is possible to increase the output frequency without changing the switching frequency, taking advantage of the complementarity of the different constituent submodules [1]. Also, given the modular concept, it is relatively easy to adapt or replace any damaged module. With the creation of redundant states and auxiliary submodules, it is possible to obtain a more fault tolerant system. In this way, continuous operation of the system is guaranteed [10, 11]. Finally, the modularity and scalability of the MMCC allow meeting any voltage level requirements [1, 5–8].

The MMCC became the most attractive MLC topology for high voltage DC transmission systems (HVDC) [4, 5, 12, 13], medium voltage drives [4, 13], active filters [4], integration with renewable energy sources [4, 9, 13, 14] and energy storage systems (ESS) [13, 14], and electrical railway systems [14, 15].

The MMCC is mentioned several times in the literature. In [16] several topologies and control strategies for MMCC with a power grid connection with a large-scale solar photovoltaic (PV) system interface are analyzed. In turn, in [17] it is presented a connection between a battery ESS and an MMCC through a non-isolated DC-DC converter. In [13] the MMCC is reviewed in respect to the submodule and overall topologies, mathematical modeling, control methods and modulation techniques. The power losses with the incorporation of advanced wide-bandgap power devices, such as Silicon Carbide (SiC) and Gallium Nitride (GaN) is also presented. Additionally, in [18] it is presented a study about the PWM techniques to a MMCC and their impact on the MLC harmonic

pollution, efficiency and ripple synthesized across its capacitors. In [1] it is presented a comparative analysis based on computer simulations of the different PWM techniques to an MMCC with 4 full bridges. In this analysis, it is demonstrated that the phase-shift carriers (PSC) and the phase-shift disposition (PSD) allow the synthesis of an output waveform with a low THD ratio. When applying the PSC PWM technique in a hybrid MMCC based on the half-bridge and full-bridge submodules, undesirable harmonics on the output voltage and uneven loss distributions between the submodules arise. To deal with these issues an improved PSC PWM technique is presented in [19]. Also, in [20] it is demonstrated that the use of a hybrid modulation technique could be the most indicated when the MMCC has a lower number of submodules due to the extra switching losses with the increase of the submodules.

Despite its numerous advantages, the MMCC presents some challenges from the hardware and control system point of view, such as: (i) the complex structure because of the need to manage a large number of switching signals; (ii) the need to measure several voltages and currents through sensors, which contributes to an enormous exchange of data at each sampling; (iii) the difficulty in keeping the DC-bus capacitor voltages balanced as well as the potential increase in energy losses due to circulating currents [4, 20]; it is not the case in the present application.

An existing solution in the literature of an MMCC consists of the parallel association of different full-bridge power electronic converters in parallel, thus allowing the same DC bus to be shared. A transformer is connected to the output of each full-bridge, the secondary winding being connected to the adjacent transformer. The transformation ratio can be different between transformers, thus increasing the input voltage as well as increasing the number of levels that can be synthesized. In the literature, there are some projects related to this topology. However, there is a research gap that allows the correct design of transformers, as well as a methodology that helps to create a more realistic simulation model based on the parameters measured in a real transformer.

In [21–27] different approaches are presented, with different numbers of voltage levels, control techniques and power levels. However, no further information regarding transformers and their sizing is provided. Additionally, the methodology for determining the simulation model parameters is not explicit. In turn, in [28] a switching technique for power balancing between submodules is proposed. In [29] they show a solution composed of 4 cascade transformers, where some transformer parameters are presented. However, the methodology used to determine the parameters of the transformers is not presented, nor is information regarding the sizing of the transformers disclosed. However, the parameters of the transformers used in simulation do not support the values used experimentally. In [30] an analysis of the existing state-of-the-art methodologies for the design of cascaded transformers is presented. In the end, a sizing methodology is proposed, which is compared with the conventional methodology. Experimental results were presented for transformers sized for 100 VA. In general, it is possible to identify a research gap that could support the development of this solution for high voltage applications as well as for higher powers. The methodology for determining the transformer parameters so that the implementation of more realistic simulation models is possible is a critical step for the correct implementation and validation of the system.

The purpose of this paper is to demonstrate the development of an MMCC composed of 3 full-bridge submodules with a common DC-bus and with cascaded power transformers. Therefore, this paper is organized as follows: Sect. 1, presents an introduction to the topic of research and explains the concept of MMCC; Sect. 2 shows the topology of MMCC used in this study; Sect. 3 describes the control algorithms implemented; Sect. 4 presents the step-by-step methodology for the MMCC analyses based on cascaded transformers, which served as the basis for the implementation of the simulation. The obtained simulation results are also presented in this section; Sect. 5 shows the experimental results of the MMCC; finally, in Sect. 6, the main conclusions of this study as well as some suggestions for future work are presented.

## 2 Full Bridge with Cascaded Transformers Topology

In Fig. 1 is illustrates the MMCC composed of full-bridge converters with cascaded power transformers. The MMCC consists of the parallel association of three full-bridge submodules sharing the same DC-bus. The output of each submodule connects to the primary side of a power transformer, while the secondary side is connected in series with the adjacent transformers [16]. In this study, these power transformers have a transformer ratio of 1:1 and are used to create the multilevel feature, since there is only one DC-bus.

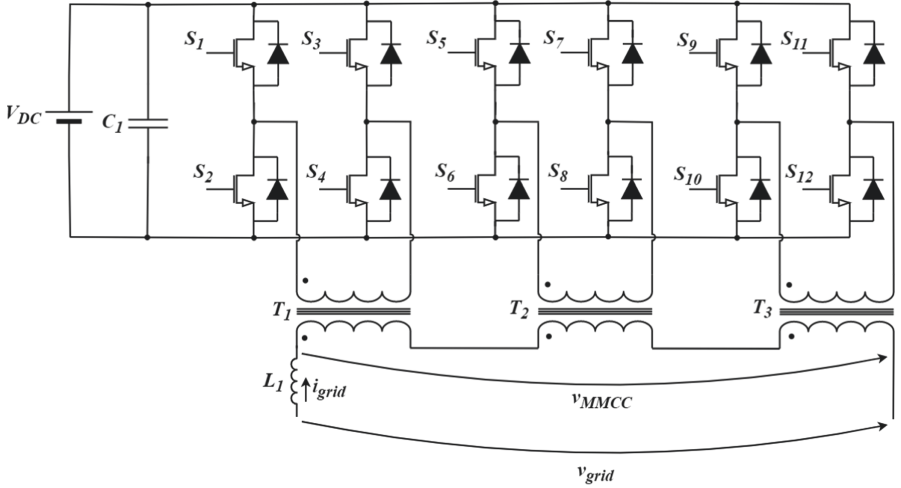


**Fig. 1.** MMCC composed of full-bridge with cascaded transformers and common DC-bus.

Considering that exists  $N$  submodules on the MMCC, by adding the voltages of each secondary winding of adjacent transformers, the number of obtained voltage levels is given by the Eq. (1).

$$N_L = 2N + 1 \quad (1)$$

For this topology, it is necessary  $4N$  power semiconductors,  $N$  transformers, and only one voltage source. It should be noted that, due to the versatility of changing the transformers

transformation ratios, it is possible to obtain different output voltage levels even with few submodules [1]. A maximum of  $3^N$  output voltage levels can be obtained, with  $N$  being the number of submodules connected in parallel. For example, in a topology with three submodules, it would be possible to obtain 27 voltage levels at the output by applying transformers with 1:1, 1:3 and 1:9 ratios [16]. However, it is necessary to implement a space vector modulation (SVM) control algorithm, as presented in [4, 7, 16, 31]. Additionally, each submodule would contribute with different powers, losing the concept of modularity.

Sharing a single DC-bus between the different submodules facilitates the control algorithms as well as the integration of other power converters. These power converters could be interfaced with an ESS or renewable energy source. From an implementation point of view, the use of only one DC-bus and the existence of a common reference for fully controlled power semiconductors make the implementation easier [1, 10]. Furthermore, this topology makes it possible to synthesize an output sinusoidal current at lower switching frequencies [16]. In fact, with the increase in the number of submodules, it is possible to reduce the switching frequency of semiconductors and the output presents less harmonic distortion [11]. This increase further reduces the value of  $dv/dt$ , mitigating the problems associated with electromagnetic interference [32].

Due to the use of a power transformer for each submodule added, the system implementation costs may be higher [9, 16]. However, it is possible to use medium-frequency transformers. These allow the integration of power semiconductors with high switching frequencies which enable the use of smaller passive filters. Additionally, the volume, weight, and implementation costs would be lower compared to low-frequency transformers [10]. Although high-frequency increases switching losses and the skin effect, it is possible to reduce losses in the passive elements [10]. Another drawback of the use of transformers in this topology is that they are not suitable for variable frequency applications [9]. Another aspect to consider is the voltage drop in each semiconductor. Considering  $N$  the number of submodules of the MMCC and  $V_{CE}$  the voltage drop in each power semiconductor, the total voltage drop in the power converter can be expressed by Eq. (2). The multiplication by 2 is explained by the fact that in a full-bridge submodule 2 semiconductors are simultaneously in conduction. As an example, considering the typical  $V_{CE\_SAT} = 3.3$  V on the SKM 100GB125DN Insulated Gate Bipolar Transistor (IGBT) module of the Semikron and 3 submodules, a total voltage drop of 19.8 V is obtained.

$$\sum V_T = 2NV_{CE} \quad (2)$$

### 3 Control Algorithms

The control algorithms of MMCC that interface with the power grid need to be synchronized with the fundamental component for an accurate and efficient operation. This synchronization algorithm must detect the signal phase as quickly as possible and the synchronization process must be continuously updated, to increase efficiency [33]. The synchronization technique used in this study was the Enhance Phase Locked Loop (EPLL), described in [33]. The EPLL can detect the phase and amplitude of the

fundamental component of a given input signal. The output signal is sinusoidal and in phase with the fundamental component of the input signal, even if it contains harmonics. Multiplying the unitary sinusoidal signal,  $pll$ , by the amplitude value,  $A$ , is possible to obtain a signal,  $v_{pll}$ , with the same phase and amplitude of the input signal fundamental component. The biggest advantage of the EPLL is the fast response to disturbances and the high rejection of the harmonic content [33]. In Fig. 2 is shown the diagram of the implemented EPLL algorithm. In the digital implementation of the EPLL the integrals were replaced by summations.

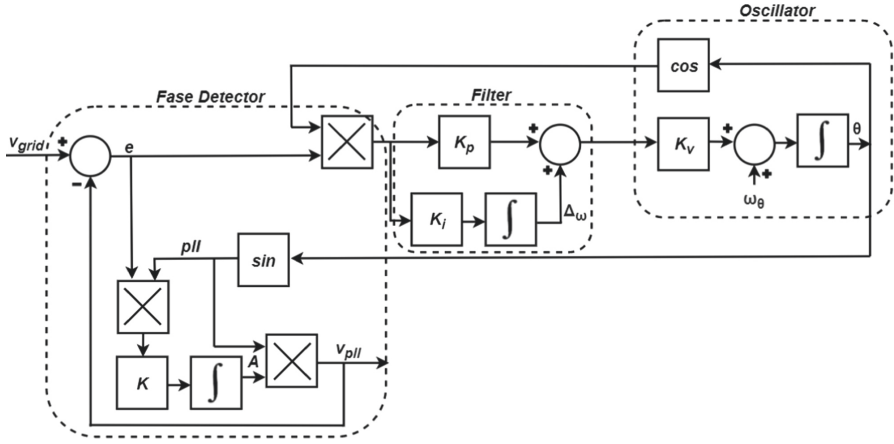


**Fig. 2.** Diagram of the implemented EPLL algorithm.

In this study, the main purpose of the MMCC is to inject energy into the power grid. Therefore, the MMCC will have the function of synthesizing a sinusoidal current in phase opposition with the power grid voltage, thus with unitary power factor. The reference current,  $i^*$ , is obtained by multiplying the desired amplitude value by the unitary sinusoidal signal,  $pll$ , resulted from the EPLL algorithm. The amplitude of the current reference depends on the power reference, and its value is given by the division between twice the power reference,  $P^*$ , and the peak value of the voltage grid,  $\hat{V}_{pk}$ , constructed using the EPLL algorithm. That said, the calculation of the reference current is depicted in Eq. (3) which is similar to the presented in [34] and in [35].

$$i^* = \frac{2P^*}{\hat{V}_{pk}} * pll \quad (3)$$

After calculating the  $i^*$  it is necessary to control the output current of the MMCC,  $i_{grid}$ , through power electronics semiconductors, specifically, through IGBT devices used in this study. For this purpose, a Proportional Integral (PI) current control algorithm and a PWM modulation technique was used, as shown in the block diagram presented in Fig. 3. Initially, the difference between  $i^*$  and  $i_{grid}$  results in an error value, *error*. This error value is then used in the PI current control algorithm to produce a command voltage,  $v_{control}$ . This command voltage establishes the modulating wave in the PWM technique.

Before the modulation process takes place and, to avoid undesirable operations, the command voltage is delimited between two pre-defined values. Regarding the PWM technique, in [1] it is demonstrated that the PSC allows the synthesis of an output waveform with a low THD ratio and is easy to implement in a Digital Signal Controller (DSC) platform, namely in the Texas Instruments C2000 platform utilized in the MMCC prototype. Therefore, the PSC was adopted to be implemented in the control system of the MMCC prototype. Finally, the modulation technique triggers the respective IGBT devices ( $S_1, \dots, S_n$ , where  $n$  is the total number of IGBT devices).

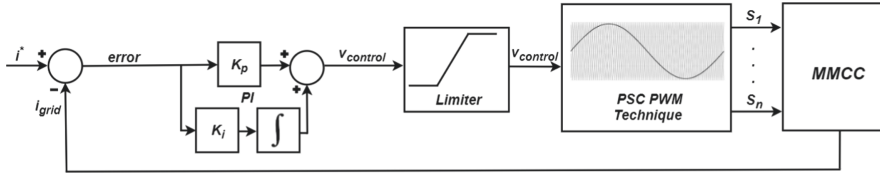


Fig. 3. Block diagram of current control used in the MMCC.

## 4 Simulation Results

In this section, the simulation results of the MMCC topology implemented are presented and analyzed. These simulations were performed in PSIM software. To obtain realistic results it is important to get an accurate model of the transformer, which is a key component in the studied topology. The transformer used in the tests has a nominal voltage of 230 V, a nominal power of 500 VA and a transformation ratio of 1:1. Considering the equivalent model of a transformer presented in Fig. 4 is important to consider:

- $R_P$  the electrical resistance of the primary winding;
- $R_S$  the electrical resistance of the secondary winding;
- $L_P$  the leakage inductance of the primary winding;
- $L_S$  the leakage inductance of the secondary winding;
- $L_M$  the magnetizing inductance.

To obtain a more realistic transformer model to use in the simulation, an LCR bridge equipment, with the references 3532-50LCR HiTESTER from the manufacture Hioki, was used to measure the transformer inductances. At this stage, was necessary to measure with the windings in series (terminal  $b$  connected to terminal  $c$  and measured from  $a$  to  $d$ ) and anti-series (terminal  $b$  connected to terminal  $d$  and measured from  $a$  to  $c$ ). When measure with the winding in series, a value of 4.9 H was obtained. On the other hand, when measured with the winding in anti-series, a value of 3.6 mH was obtained.

The measurement of these two inductances allows the calculation of the self-inductance of the primary winding ( $L_1$ ), the self-inductance of the secondary winding ( $L_2$ ), and the mutual inductance between the primary and secondary windings ( $M$ ), through Eq. (4) and Eq. (5). Since the primary and secondary windings have the

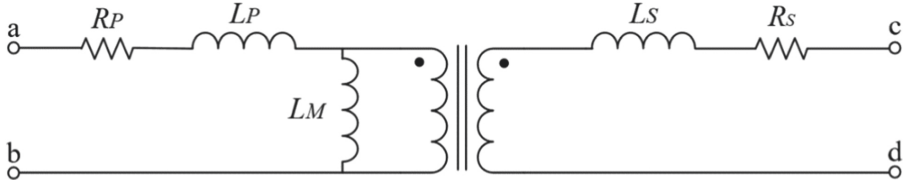


**Fig. 4.** Equivalent model of the transformer used in this study.

same number of turns,  $L_1$  is approximately equal to  $L_2$  and thus, in the equations, the self-inductance of the windings was represented by  $L$ , as represented in Eq. (6) [36].

$$L_{series} = 2L + 2M = 4.9 \text{ H} \quad (4)$$

$$L_{anti-series} = 2L - 2M = 3.6 \text{ mH} \quad (5)$$

$$L = L_1 = L_2 \quad (6)$$

To obtain the values of the inductances  $L$  and  $M$ , it is necessary to solve a system of equations with Eqs. (4) and (5). Therefore, by substituting the  $L$  of Eq. (5) into Eq. (4), it is possible to obtain the Eq. (7). Thus, the value of  $M$  can be calculated. Having the value of  $M$ , the value of  $L$  can be easily obtained by substituting the value of  $M$  in Eq. (8).

$$M = \frac{L_{series} - L_{anti-series}}{4} = 1.224 \text{ H} \quad (7)$$

$$L = \frac{L_{series} + 2M}{2} = 1.226 \text{ H} \quad (8)$$

The self-inductance of the windings,  $L_1$  and  $L_2$ , represents the electromotive force induced in each winding due to the magnetic field produced by the current in the winding itself. The mutual inductance between the windings,  $M$ , represents the electromotive force induced in the primary winding due to the magnetic field produced by the current in the secondary winding [36]. Once have been calculated the self-inductance of the windings and the mutual inductance between the windings, it is possible to calculate the coupling coefficient between the windings,  $k$ , through Eq. (9). The  $k$  is a value between 0 and 1. When this coefficient has the value of 0 it means that there is no magnetic coupling between the primary and the secondary winding. When the coefficient is 1, the coupling is ideal, that is, all the magnetic flux produced by the primary winding links the secondary winding, and vice versa. Thus, the magnetic flux is equal throughout the magnetic circuit [36]. To highlight that the obtained value of  $k$  was close to 1, as desired.

$$k = \frac{M}{\sqrt{L_1 L_2}} = 0.999 \quad (9)$$

Finally, after calculating the coupling coefficient between the windings, it is possible to calculate the leakage inductances,  $L_P$  and  $L_S$ , as well as the magnetization inductance,



$L_M$ , present in the equivalent transformer model, through Eq. (10), Eq. (11), and Eq. (12) [36].

$$L_P = (1 - k)L_1 = 1.8 \text{ mH} \quad (10)$$

$$L_S = (1 - k)L_2 = 1.8 \text{ mH} \quad (11)$$

$$L_M = kL_1 = 1.22 \text{ H} \quad (12)$$

To obtain the values of the winding resistances,  $R_P$  and  $R_S$ , a precision multimeter equipment was used, with the reference 34450 A from the manufacture Keysight Technologies. For the resistance  $R_P$ , the transformer terminals  $a$  and  $b$  were measured, leaving terminals  $c$  and  $d$  in an open circuit. For resistance  $R_S$  the transformer terminals  $c$  and  $d$  were measured, leaving terminals  $a$  and  $b$  in an open circuit. The obtained value of resistance  $R_P$  was  $3.1 \text{ } \Omega$  and the value of resistance  $R_S$  was  $3.7 \text{ } \Omega$ , all measured at a frequency of  $1 \text{ kHz}$ .

After performing these measurements and calculations, it is now possible to place these parameters in the simulation model to be able to obtain results closer to reality. Table 1 presents the values of the main components used in the computational simulation of the studied topology. The values of the components used were obtained in such a way as to be the closest to the ones used in the laboratory prototype. Moreover, the power grid voltage presents the harmonic content presented in the Table 2.

The implementation and respective simulation of the EPLL algorithm for power grid voltage synchronization were carried out, and the obtained simulation results are shown in Fig. 5. As it can be seen, the EPLL algorithm quickly synchronizes with the frequency and phase of the power grid voltage fundamental component and determines the amplitude in a maximum of 4 power grid cycles. In this way, the dynamic response of the algorithm is verified, which can detect and monitor voltage variations in the power grid. Additionally, despite the power grid voltage has harmonic content, the EPLL waveform presents a residual THD value. Once concluded, the correct functioning of the EPLL algorithm allows the synchronization of the converter with the power grid, which provides a dynamic response to the system.

In Fig. 6 is shown the output voltage waveform of the MMCC. In Fig. 6(a) using an ideal transformer and in Fig. 6(b) using an equivalent model of real transformer. As can be seen in Fig. 6(a), the use of three submodules in series allows, as predicted, the existence of seven voltage levels at the output. In a real application, transformer windings contain inductances and resistances, which cause losses, as seen in Fig. 4. The influence of this parameters can make it difficult to visualize the output voltage levels because of the slower  $dv/dt$  response. Even so, the presence of inductances in the transformer windings allows obtaining a voltage waveform close to a sinusoidal (Fig. 6(b)). Nevertheless, it should be noted that with the ideal simulation model, it would be possible to obtain an MMCC output voltage with a maximum value of  $180 \text{ V}$ , three times the DC-bus voltage. On the other hand, with a real simulation model, the voltage drops in the IGBT devices and in the magnetic elements is considerable to the point that only a maximum value of  $90 \text{ V}$  can be obtained. Note that the MMCC based on cascade transformers should start operating at  $90^\circ$  or  $-90^\circ$ . This is due to the fact that the variation of the magnetic flux

**Table 1.** Specification of the simulation parameters.

Description	Variables	Value	Units
Coupling coil	$L_I$	4	mH
Power grid voltage	$v_{grid}$	60	V <sub>RMS</sub>
DC-bus voltage	$V_{DC}$	60	V
Power grid line inductance	$L_z$	100	$\mu$ H
Power grid line resistance	$R_z$	2	m $\Omega$
Resistance of the primary winding of the transformer	$R_P$	3.1	$\Omega$
Resistance of the secondary winding of the transformer	$R_S$	3.7	$\Omega$
Inductance of the primary winding of the transformer	$L_P$	1.8	mH
Inductance of the secondary winding of the transformer	$L_S$	1.8	mH
The magnetizing inductance	$L_M$	1.22	H
Transformers turns-ratio	N	1:1	–
IGBT saturation voltage	$V_{CE}$	3.3	V
IGBT collector-emitter resistance	$r_{CE}$	8.1	m $\Omega$
IGBT diode threshold voltage	$V_F$	2	V
IGBT diode resistance	$r_F$	12	m $\Omega$
IGBT switching frequency	$f_w$	1	kHz
Sampling frequency	$f_s$	50	kHz

**Table 2.** Main harmonic components in the power grid voltage [37].

Harmonic order	Amplitude (V <sub>RMS</sub> )	Phase (°)
1	60	0
3	0.26	95
5	0.15	135
7	2.18	44
9	0.42	–147
11	0.97	–134
13	0.05	29
15	0.07	–20
THD	4.1%	

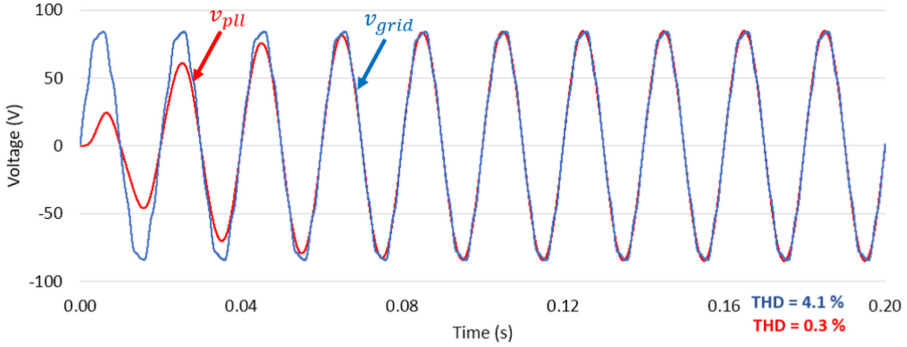


**Fig. 5.** Simulation result of the EPLL synchronism: power grid voltage,  $v_{grid}$ , and pll signal,  $v_{pll}$ .

does not present an average value of zero at each switching period. In this topology, the variation of the magnetic flux presents an almost sinusoidal wave along the period of the fundamental component of the output signal. If the start is different from  $90^\circ$  or  $-90^\circ$ , the variation of the magnetic flux will present an average value, being able to saturate the ferromagnetic core.

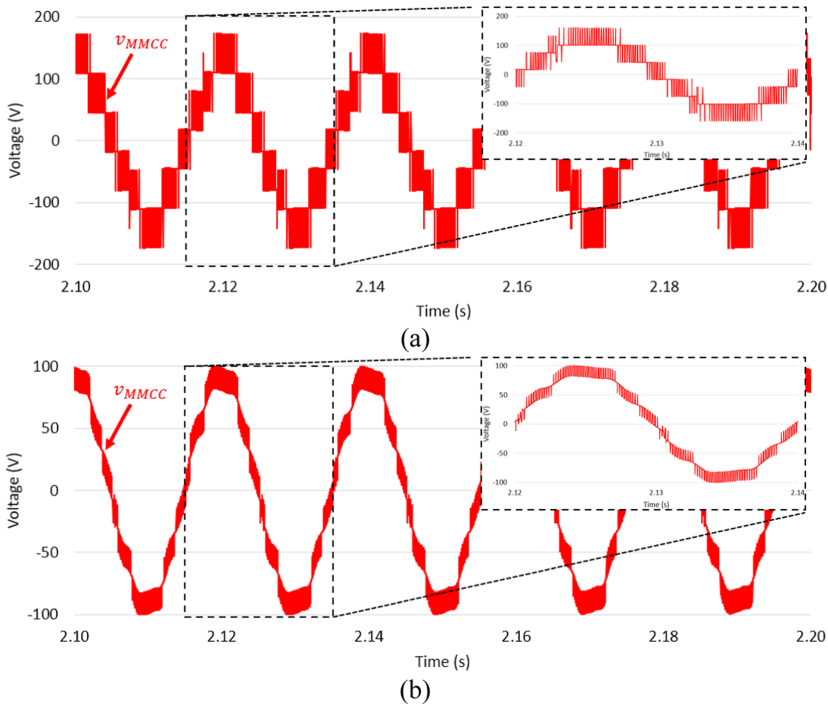


**Fig. 6.** Simulations results of the MMCC injecting energy into the power grid: (a) output voltage waveform,  $v_{MMCC}$ , with ideal transformers model; (b) output voltage waveform,  $v_{MMCC}$ , with real transformers model.

After completing the system initialization processes, the MMCC control is fully functional within 0.5 s, as is a highlight in Fig. 7. The MMCC will have the ability to inject energy into the power grid, depending on the  $P^*$  value. Therefore, with the introduction of  $P^*$  value, the active power injected into the power grid,  $P_{grid}$ , must follow the reference,  $P^*$ , as shown in Fig. 7.

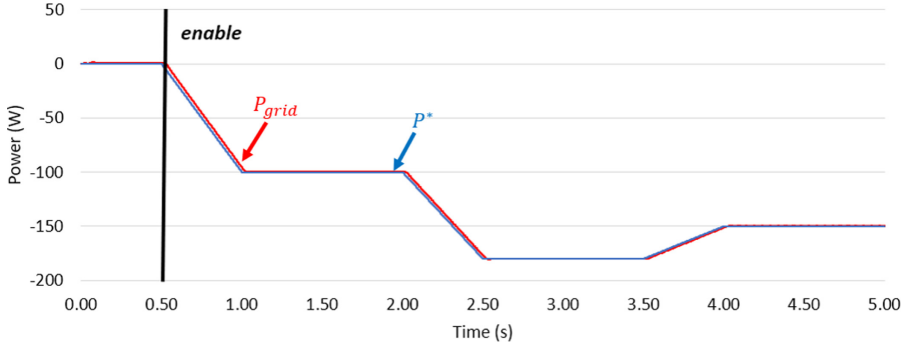


**Fig. 7.** Simulations results of the MMCC injecting energy into the power grid: active power injected into the power grid,  $P_{grid}$ , and the power reference,  $P^*$ .

Analyzing Fig. 8, it is possible to see that the synthesized current,  $i_{grid}$ , follows the reference current,  $i^*$ . It can be concluded the correct operation of the current control algorithm implemented, resulting in grid current,  $i_{grid}$ , with low harmonic distortion (THD% = 2.5%). Nevertheless, to highlight that the PI current control algorithm allows the MMCC to synthesize a sinusoidal current,  $180^\circ$  lag in relation to the power grid voltage, injecting energy into the power grid.

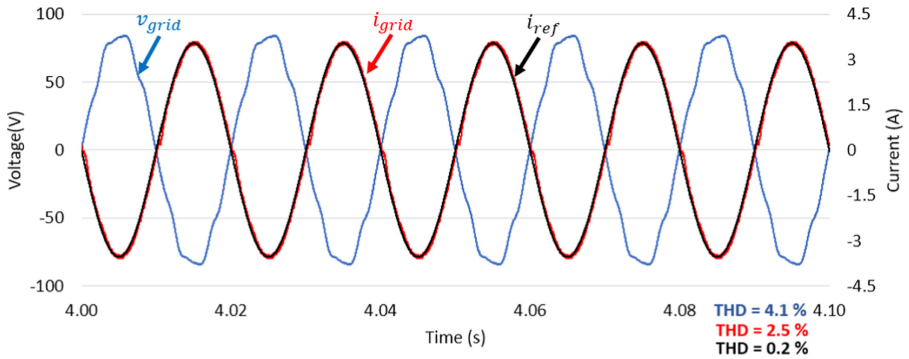


**Fig. 8.** Simulations results of the MMCC injecting energy into the power grid: power grid voltage,  $v_{grid}$ , reference current,  $i_{ref}$ , and grid current,  $i_{grid}$ .

## 5 Experimental Results

Once the computer simulations have been validated, all the hardware was assembled, highlighting the control system and the power system. Figure 9 shows a general overview of the laboratory workbench, where the hardware was assembled and tested. In this section are presented some experimental results of the MMCC composed of full-bridge with cascaded power transformers implemented.

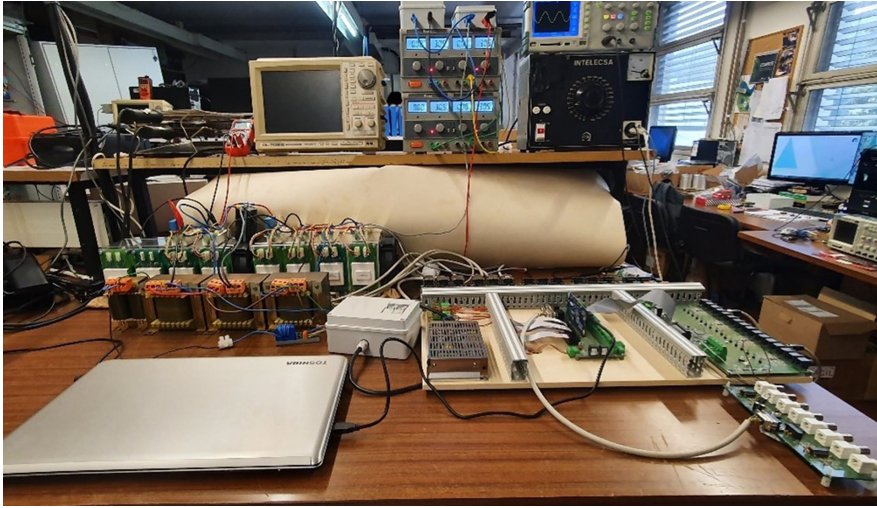


**Fig. 9.** View of the hardware assembled in the laboratory workbench.

Table 3 shows the specification of the operation conditions of the laboratory prototype implemented for the experimental tests. The DSC platform used was the Control Card-F28379D from Texas Instruments.

The PWM peripheral was configured in the DSC with  $3 \mu\text{s}$  of dead time to avoid a short circuit of the DC-bus voltage source caused by the simultaneous conduction of semiconductors in the same arm of the full-bridge submodule. Other parameters were also configured, such as the time period and phase offset of the carrier wave in each arm of the full-bridge submodules, to obtain the desired PSC PWM technique. That is, six carrier waveforms were implemented with a frequency equal to 1 kHz and out of phase with each other by  $60^\circ$ .

To produce a sinusoidal current in phase opposition relativity to the power grid voltage, it is necessary to produce a signal synchronized with the fundamental component of the power grid voltage, as already mentioned. Thus, the synchronism of the EPLL signal algorithm with the power grid voltage is shown in Fig. 10, based on the algorithm used in the computational simulations. Note that the  $v_{grid}$  and  $v_{pll}$  are visualized using a Digital-Analog Converter (DAC) with the reference TLV5610 by the manufacturer Texas Instruments with 0.016 V/V scale.

In an ideal scenario, the output voltage of the MMCC would be 3 times the voltage on the DC-bus ( $3 * 60 \text{ V}$ ). However, considering the voltage drops in the IGBT devices,

**Table 3.** Specification of the MMCC main components and operation conditions.

Description	Variables	Value	Units
Coupling coil	$L_I$	4	mH
DC-bus capacitor	$C_I$	1	mF
DC-bus voltage	$V_{DC}$	60	V
Power grid voltage	$v_{grid}$	60	V <sub>RMS</sub>
Transformers turns-ratio	N	1:1	–
IGBT switching frequency	$f_w$	1	kHz
Sampling frequency	$f_s$	50	kHz
Current sensor	CYHCS-B6-100A		
Voltage sensor	CYHVS5-25A		
IGBT	SKM 100GB125DN <sup>a</sup>		

<sup>a</sup>Although used in the experimental results this device is oversized for this application

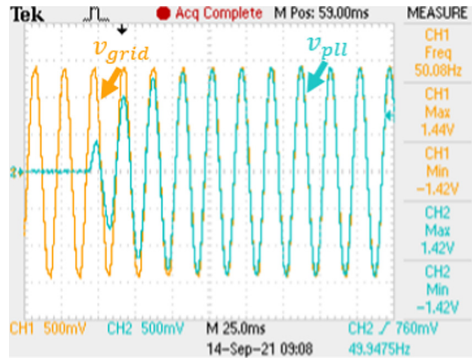


**Fig. 10.** Experimental results of the EPLL synchronism: power grid voltage,  $v_{grid}$ , and output signal,  $v_{pll}$ .

and in the low frequency transformers, the output voltage presents a similar waveform to the obtained on the real model simulations. Analyzing Fig. 11 it can be concluded that the MMCC can synthesize all the expected voltage levels, with a maximum voltage variation up to 106 V and minimum of  $-118$  V.

To inject energy into the power grid, the current synthesized by the MMCC must be in phase opposition relativity to the power grid voltage. Moreover, the output voltage of the MMCC must be higher than the peak value of the power grid voltage. The experimental results obtained for the injection of energy into the power grid with the variation of the power reference from 80 W to 110 W are shown in Fig. 12.

A power reference of 80 W and 100 W was given to the MMCC. Considering the power grid voltage, the control system determined a reference current of  $1.85 A_{peak}$  and  $2.3 A_{peak}$ , respectively. The results presented in Fig. 13 prove the correct functioning of

the MMCC, where  $i_{grid}$  follows  $i_{ref}$ . Note that the  $i_{ref}$  and  $i_{grid}$  are visualized using a DAC with a 1 V/A scale.

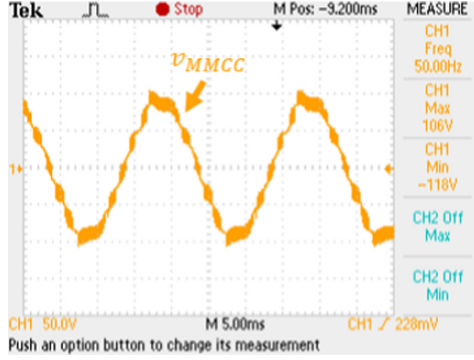


**Fig. 11.** Experimental results of the MMCC: output voltage waveform,  $v_{MMCC}$ .

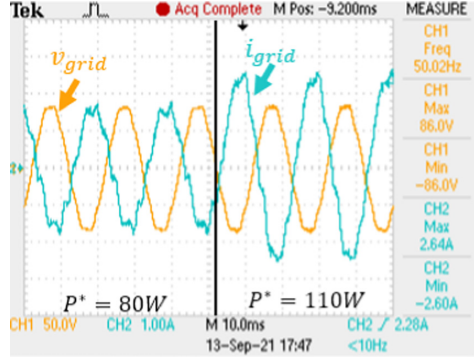


**Fig. 12.** Experimental results of the MMCC while injecting energy into the power grid: power grid voltage,  $v_{grid}$ , and grid current,  $i_{grid}$ .

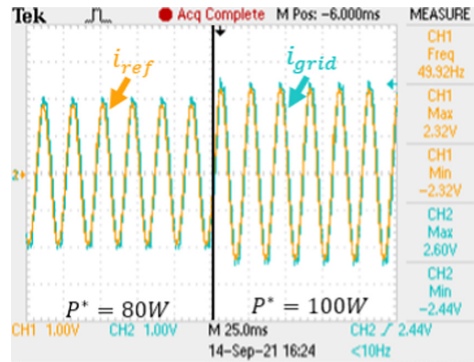


**Fig. 13.** Experimental results of the MMCC while injecting energy into the power grid: reference current,  $i_{ref}$ , and grid current,  $i_{grid}$ .

## 6 Conclusions

This paper presents the development of a Modular Multilevel Cascade Converter (MMCC) composed of full-bridge submodules with a common DC-bus and with low frequency cascaded transformers. The MMCC was first validated based on computer simulations, with the entire methodology being presented step by step as well as the control algorithms. Regarding the simulation model, the parameters of the real were used, namely in the transformers equivalents model. As such, it was necessary to carry out experimental tests and measurements in order to obtain the important parameters for the implemented model. The entire procedure is presented in detail in order to be easily replicable by other researchers. The simulation model was validated based on the experimental results, obtaining experimental results similar to those of simulation.

Regarding the operation of the MMCC, it was possible to prove the correct functioning of the system, validating the control algorithms implemented either in simulation or in the laboratory prototype. In the experimental tests the synthesized output current follows the reference, presenting low ripple and THD, being very similar to the results achieved in simulation.

As the main technical conclusions of the work, it can be concluded that the low-frequency transformers generate audible noise due to vibrations during the operation of the MMCC. In order to maximize the system efficiency, the inclusion of LCL filters at the input of each transformer, in order to apply a sinusoidal waveform to each low-frequency transformer would be studied. This solution could increase transformer efficiency despite increasing losses in passive filters, since they would have to be replicated depending on the number of submodules added. This solution, instead of adding square waves, presenting a stair output waveform, would add sine waves, which could reduce the output harmonic spectrum. However, this approach eliminates one of the advantages of the MMCC, which is the frequency multiplication applied to the output filter. The frequency multiplication could aid to reduce the weight, volume, and cost of the final solution. Another solution would be the study, design and development of medium-frequency transformers for the specific application. The use of amorphous ferromagnetic materials would present an added value since they allow a higher magnetic flux density, allowing operation with higher switching frequencies, as well as it would be possible to obtain a more compact solution.

It is possible to highlight that there is a research gap in the MMCC topology based on cascade transformers. Despite its potential, presenting a common DC-bus, which facilitates not only control algorithms but also the integration of other interfaces, such as renewables energies or energy storage systems, also presents some implementation challenges. Since the solution of cascade transformers with full-bridges allows the bidirectional flow of energy, this characteristic would be more widely explored if there were an interface with bidirectional energy system, such as in the case of an energy storage system. The interface with renewable energy sources, despite its unidirectional energy flow, would appear as an additional interface.

**Acknowledgements.** This work has been supported by FCT – Fundação para a Ciência e Tecnologia with-in the Project Scope: UIDB/00319/2020. This work has been supported by the FCT Project QUALITY4POWER PTDC/EEI-EEE/28813/2017, and by the FCT Project DAIPESEV



PTDC/EEI-EEE/30382/2017. Mr. Luis A. M. Barros is supported by the doctoral scholarship PD/BD/143006/2018 granted by the Portuguese FCT foundation.

## References

1. Barros, L.A.M., Tanta, M., Martins, A.P., Afonso, J.L., Pinto, J.G.: Submodule topologies and PWM techniques applied in modular multilevel converters: review and analysis. In: Afonso, J.L., Monteiro, V., Pinto, J.G. (eds.) SESC 2020. LNICSSITE, vol. 375, pp. 111–131. Springer, Cham (2021). [https://doi.org/10.1007/978-3-030-73585-2\\_8](https://doi.org/10.1007/978-3-030-73585-2_8). ISBN 978-3-030-73584-5
2. Steimel, A.: Electric traction-motive power and energy supply: basics and practical experience. Oldenbourg Industrieverlag (2008). ISBN 978-3-8356-3132-8
3. Sharifabadi, K., Harnefors, L., Nee, H.-P., Norrga, S., Teodorescu, R.: Design, Control, and Application of Modular Multilevel Converters for HVDC Transmission Systems. Wiley (2016). ISBN 9781118851548
4. Perez, M.A., Bernet, S., Rodriguez, J., Kouro, S., Lizana, R.: Circuit topologies, modeling, control schemes, and applications of modular multilevel converters. *IEEE Trans. Power Electron.* **30**(1), 4–17 (2014). <https://doi.org/10.1109/TPEL.2014.2310127>, ISSN:0885-8993
5. Debnath, S., Qin, J., Bahrani, B., Saeedifard, M., Barbosa, P.: Operation, control, and applications of the modular multilevel converter: a review. *IEEE Trans. Power Electron.* **30**(1), 37–53 (2014). <https://doi.org/10.1109/TPEL.2014.2309937>, ISSN:0885-8993
6. Liao, J., Corzine, K., Ferdowsi, M.: A new control method for single-DC-source cascaded H-bridge multilevel converters using phase-shift modulation. In: 2008 Twenty-Third Annual IEEE Applied Power Electronics Conference and Exposition, pp. 886–890 (2008). <https://doi.org/10.1109/APEC.2008.4522825>. ISBN 978-1-4244-1873-2
7. Brenna, M., Foiadelli, F., Zaninelli, D.: Electrical Railway Transportation Systems. Wiley (2018). ISBN 978-1-119-38680-3
8. Zhao, C., Li, Y., Li, Z., Wang, P., Ma, X., Luo, Y.: Optimized design of full-bridge modular multilevel converter with low energy storage requirements for HVDC transmission system. *IEEE Trans. Power Electron.* **33**(1), 97–109 (2017). <https://doi.org/10.1109/TPEL.2017.2660532>. ISSN:1941-0107
9. Yellasisiri, S., Panda, A.: Performance of cascade multilevel H-Bridge inverter with single DC source by employing low frequency three-phase transformers, pp. 1981–1986 (2010). <https://doi.org/10.1109/IECON.2010.5675291>
10. Barros, L.A., Tanta, M., Martins, A.P., Afonso, J.L., Pinto, J.: Opportunities and challenges of power electronics systems in future railway electrification. In: 2020 IEEE 14th International Conference on Compatibility, Power Electronics and Power Engineering (CPE-POWERENG), vol. 1, pp. 530–537 (2020). <https://doi.org/10.1109/CPE-POWERENG48600.2020.9161695>. ISSN 2166-9545
11. Xu, Q., et al.: Analysis and comparison of modular railway power conditioner for high-speed railway traction system. *IEEE Trans. Power Electron.* **32**(8), 6031–6048 (2016). <https://doi.org/10.1109/TPEL.2016.2616721>. ISSN 0885-8993
12. Dekka, A., Wu, B., Fuentes, R.L., Perez, M., Zargari, N.R.: Evolution of topologies, modeling, control schemes, and applications of modular multilevel converters. *IEEE J. Emerg. Sel. Top. Power Electron.* **5**(4), 1631–1656 (2017). <https://doi.org/10.1109/JESTPE.2017.2742938>. ISSN 2168-6785
13. Wang, Y., Aksoz, A., Geury, T., Ozturk, S.B., Kivanc, O.C., Hegazy, O.: A review of modular multilevel converters for stationary applications. *Appl. Sci.* **10**(21), 7719 (2020). <https://doi.org/10.3390/app10217719>

14. Feng, J., Chu, W., Zhang, Z., Zhu, Z.: Power electronic transformer-based railway traction systems: challenges and opportunities. *IEEE J. Emerg. Sel. Top. Power Electron.* **5**(3), 1237–1253 (2017). <https://doi.org/10.1109/JESTPE.2017.2685464>. ISSN 2168-6777
15. Tanta, M., Barros, L.A., Pinto, J., Martins, A.P., Afonso, J.L.: Modular multilevel converter in electrified railway systems: applications of rail static frequency converters and rail power conditioners. In: 2020 International Young Engineers Forum (YEF-ECE), pp. 55–60 (2020). <https://doi.org/10.1109/YEF-ECE49388.2020.9171814>. ISBN 978-1-7281-5679-8
16. Latran, M.B., Teke, A.: Investigation of multilevel multifunctional grid connected inverter topologies and control strategies used in photovoltaic systems. *Renew. Sustain. Energy Rev.* **42**, 361–376 (2015). <https://doi.org/10.1016/j.rser.2014.10.030>
17. Cao, W., Xu, Y., Han, Y., Ren, B.: Comparison of cascaded multilevel and modular multilevel converters with energy storage system. In: 2016 IEEE 11th Conference on Industrial Electronics and Applications (ICIEA), pp. 290–294 (2016). <https://doi.org/10.1109/ICIEA.2016.7603596>. ISBN 978-1-4673-8645-6
18. Antonio-Ferreira, A., Collados-Rodriguez, C., Gomis-Bellmunt, O.: Modulation techniques applied to medium voltage modular multilevel converters for renewable energy integration: a review. *Electr. Power Syst. Res.* **155**, 21–39 (2018). <https://doi.org/10.1016/j.epsr.2017.08.015>
19. Lu, S., Yuan, L., Li, K., Zhao, Z.: An improved phase-shifted carrier modulation scheme for a hybrid modular multilevel converter. *IEEE Trans. Power Electron.* **32**(1), 81–97 (2016). <https://doi.org/10.1109/TPEL.2016.2532386>. ISSN 1941-0107
20. Marquez, A., Leon, J.I., Vazquez, S., Franquelo, L.G., Perez, M.: A comprehensive comparison of modulation methods for MMC converters. In: IECON 2017–43rd Annual Conference of the IEEE Industrial Electronics Society, pp. 4459–4464 (2017). <https://doi.org/10.1109/IECON.2017.8216768>. ISBN 978-1-5386-1127-2
21. Song, S.G., Kang, F.S., Park, S.-J.: Cascaded multilevel inverter employing three-phase transformers and single DC input. *IEEE Trans. Industr. Electron.* **56**(6), 2005–2014 (2009). <https://doi.org/10.1109/TIE.2009.2013846>. ISSN 1557-9948
22. Kang, F.-S., Park, S.-J., Lee, M.H., Kim, C.-U.: An efficient multilevel-synthesis approach and its application to a 27-level inverter. *IEEE Trans. Industr. Electron.* **52**(6), 1600–1606 (2005). <https://doi.org/10.1109/TIE.2005.858715>. ISSN 1557-9948
23. Ortúzar, M.E., Carmi, R.E., Dixon, J.W., Morán, L.: Voltage-source active power filter based on multilevel converter and ultracapacitor DC link. *IEEE Trans. Industr. Electron.* **53**(2), 477–485 (2006). <https://doi.org/10.1109/TIE.2006.870656>. ISSN 1557-9948
24. Flores, P., Dixon, J., Ortúzar, M., Carmi, R., Barriuso, P., Morán, L.: Static var compensator and active power filter with power injection capability, using 27-level inverters and photovoltaic cells. *IEEE Trans. Industr. Electron.* **56**(1), 130–138 (2008). <https://doi.org/10.1109/ISIE.2006.295791>, ISBN: 1-4244-0497-5
25. Zhou, L., Fu, Q., Li, X., Liu, C.: A novel Multilevel Power Quality Compensator for electrified railway, pp. 1141–1147 (2009). <https://doi.org/10.1109/IPEMC.2009.5157555>
26. ElGebaly, A.E., Hassan, A.E.-W., El-Nemr, M.K.: Reactive power compensation by multilevel inverter STATCOM for railways power grid. In: 2019 IEEE Conference of Russian Young Researchers in Electrical and Electronic Engineering (EIConRus), pp. 2094–2099 (2019). <https://doi.org/10.1109/EIConRus.2019.8657058>. ISBN 978-1-7281-0339-6
27. Zhou, L., Fu, Q., Li, X., Liu, C.: A novel photovoltaic grid-connected power conditioner employing hybrid multilevel inverter. In: 2009 International Conference on Sustainable Power Generation and Supply, pp. 1–7 (2009). <https://doi.org/10.1109/SUPERGEN.2009.5348154>. ISSN 2156-9681

28. Park, S.-J., Kang, F.-S., Cho, S.E., Moon, C.-J., Nam, H.-K.: A novel switching strategy for improving modularity and manufacturability of cascaded-transformer-based multilevel inverters. *Electric Power Syst. Res.* **74**(3), 409–416 (2005). <https://doi.org/10.1016/j.epsr.2005.01.005>. ISSN 0378-7796. <https://www.sciencedirect.com/science/article/pii/S0378779605000751>
29. Jahan, H., Naseri, M., Haji Esmaeili, M., Abapour, M., Zare, K.: Low component merged cells cascaded-transformer multilevel inverter featuring an enhanced reliability. *IET Power Electronics* **10** (2017). <https://doi.org/10.1049/iet-pel.2016.0787>
30. Diaz Rodriguez, J., Pabon, L., Peñaranda, E.: Novel methodology for the calculation of transformers in power multilevel converters **17**, 121–132 (2015)
31. Miura, Y., Mizutani, T., Ito, M., Ise, T.: A novel space vector control with capacitor voltage balancing for a multilevel modular matrix converter. In: 2013 IEEE ECCE Asia Downunder, pp. 442–448 (2013). <https://doi.org/10.1109/ECCE-Asia.2013.6579134>. ISBN 978-1-4799-0482-2
32. Nami, A., Liang, J., Dijkhuizen, F., Demetriades, G.D.: Modular multilevel converters for HVDC applications: review on converter cells and functionalities. *IEEE Trans. Power Electron.* **30**(1), 18–36 (2014). <https://doi.org/10.1109/TPEL.2014.2327641>. ISSN 0885-8993
33. Karimi-Ghartemani, M., Iravani, M.R.: A method for synchronization of power electronic converters in polluted and variable-frequency environments. *IEEE Trans. Power Syst.* **19**(3), 1263–1270 (2004). <https://doi.org/10.1109/TPWRS.2004.831280>, ISSN:1558-0679
34. Barros, L.A., Tanta, M., Sousa, T.J., Afonso, J.L., Pinto, J.: New multifunctional isolated microinverter with integrated energy storage system for PV applications. *Energies* **13**(15), 4016 (2020). <https://doi.org/10.3390/en13154016>, ISSN:1996-1073
35. Pinto, J., Monteiro, V., Gonçalves, H., Afonso, J.L.: Onboard reconfigurable battery charger for electric vehicles with traction-to-auxiliary mode. *IEEE Trans. Veh. Technol.* **63**(3), 1104–1116 (2013). <https://doi.org/10.1109/TVT.2013.2283531>, ISSN:1939-9359
36. Rogers, J.W., Plett, C.: *Radio Frequency Integrated Circuit Design*. Artech House (2010). ISBN 978-1580535021
37. Barros, L.A., Tanta, M., Martins, A.P., Afonso, J.L., Pinto, J.: STATCOM evaluation in electrified railway using V/V and Scott power transformers. In: *International Conference on Sustainable Energy for Smart Cities*, pp. 18–32 (2019). [https://doi.org/10.1007/978-3-030-45694-8\\_2](https://doi.org/10.1007/978-3-030-45694-8_2). ISBN 978-3-030-45693-1